JOURNAL OF MATERIALS SCIENCE 27 (1992) 374–380

Interfacial phenomenology of SiC fibre reinforced $Li_2O \cdot Al_2O_3 \cdot 6SiO_2$ glass-ceramic composites

JEN-YAN HSU, R. F. SPEYER
The New York State College of Ceramics at Alfred University, Alfred, NY 14802, USA

The microstructures of SiC fibre-reinforced $Li_2O \cdot Al_2O_3 \cdot 6SiO_2$ glass-ceramic composites with Ta_2O_5, Nb_2O_5, TiO_2 and ZrO_2 dopants were investigated. An amorphous carbon-rich layer, from 100–170 nm thick, was observed in the interfacial region between fibre and matrix. A second interfacial layer of TaC, NbC, or TiC precipitates, appeared adjacent to the C-rich layer. Low bond strength between these two interfacial layers resulted in low interfacial shear strength, and this in turn led to an increase in toughness of the composites containing 4 mol% Ta_2O_5 or Nb_2O_5 dopant. 2 mol% Ta_2O_5 dopant in this composite acted as a nucleating agent for the matrix but was not adequate to form an appreciable volume of TaC particles in the interfacial region, hence a flexural strength decrease was observed. The composite containing TiO_2 dopant exhibited low flexural strength and fracture toughness resulting from the formation of a TiC layer which had a larger coherent bond strength with the interfacial C-rich layer, and attacked the structural integrity of the fibres.

1. Introduction

Nicalon SiC fibre-reinforced glass-ceramic composites [1–6] have generated significant attention owing to their superior mechanical properties at room as well as at elevated temperatures [5, 7]. The flexural strength of these composites is three to four times larger than that of monolithic glass ceramics. This is due to the fact that applied load transfers from the matrix to the stronger and stiffer SiC fibre reinforcement [6–8]. In addition to their high moduli of rupture, the composites also have exhibited very high fracture toughness, their critical stress intensity factor, K_{IC}, values have been reported as $\sim 17\ MPa\ m^{1/2}$ [7, 8]. A fibre/matrix interfacial amorphous C-rich layer, facilitating optimal bonding coherence between the SiC fibre and matrix [9–11], has led to fibre debonding, fibre bridging, crack deflection and fibre pull-out properties, which caused a remarkable enhancement in toughness [12–14].

This interfacial C-rich layer, which formed during the composite fabrication process (hot pressing) resulted from a reaction between the fibre and matrix, $SiC + O_2 \rightarrow SiO_2 + C$ [11], whereby C was available to form a coating layer on the fibre. Excessive addition of glass network-modifiers in the silicate glass, such as Li_2O, acts to cause the above reaction to occur more violently, resulting in a CO gas release ($2C + O_2 \rightarrow 2CO$) [11, 15]. The resulting bubble-impregnated microstructure at interfacial regions, as well as in the matrix, diminished the composite's mechanical properties [7, 11]. In order to avoid the formation of this gas, a conditional network-former, such as Nb_2O_5, has been added to the matrix composition in order to buffer the fibre/matrix reactivity, and causing the development of a niobium carbide layer outside the amorphous C-rich layer [5, 9, 11]. The mechanical properties of these composites were much improved due to the formation of this second interfacial carbide layer and the elimination of gaseous bloating in the microstructure [5, 16, 17].

In previous work [8], our efforts have focused on the fabrication of composites using Nicalon SiC fibre to unidirectionally reinforce $Li_2O \cdot Al_2O_3 \cdot 6SiO_2$ glass ceramics containing various nucleating agents [18–20]. These additives also acted as dopants to create the aforementioned interfacial carbide layer. Table I indicates the compositions of glass matrices with various additives, and the mechanical properties of these composites in the as-pressed form [8]. Mechanical properties varied with matrix composition as well as hot-pressing parameters. Strength and toughness of the composites were controlled by their microstructure, especially in the interfacial regions, which in turn were closely related to the matrix composition and fabrication process. Therefore, this study focused on the microstructure of these composites by utilizing a high-resolution transmission electron microscope (TEM) with an energy dispersive spectrometry (EDS) attachment. This device was used to reveal the fibre/matrix interfacial microstructure and microchemistry and correlate it to the fabrication process and measured mechanical properties.

0022–2461/92 $03.00 + .12

TABLE I Dopants in matrix, hot-pressing conditions, flexural strength (20 tests in each set), fracture toughness, K_{IC} (5 tests in each set), with standard deviation, and interfacial shear strength between fibre and matrix of the composites fabricated in our previous work [8]

Matrix	Dopant (mol %)	Hot pressing conditions		Flexural strength (MPa)	Toughness K_{IC}(MPa $m^{1/2}$)	Interfacial shear strength (MPa)
		(MPa)	(°C)			
LAS I	Ta_2O_5/2.0	7.9	1350	630.7 ± 29.9	15.6 ± 2.7	4.0
LAS II	Ta_2O_5/4.0	7.9	1300	860.3 ± 76.3	17.0 ± 4.3	4.8
	Ta_2O_5/4.0	7.9	1350	839.8 ± 42.9	15.7 ± 2.1	5.6
LAS III	Nb_2O_5/4.0	7.9	1400	718.6 ± 61.7	14.1 ± 3.4	12.5
LAS IV	TiO_2/3.0, ZrO_2/1.0 Nb_2O_5/1.88	7.9	1350	445.0 ± 27.2	10.7 ± 2.8	23.0

2. TEM sample preparation

The as-pressed composites were cut into 3 mm diameter discs with a thickness of less than 1 mm. They were mechanically ground to about 70–80 μm thick and a basin in the centre of the disc was dimpled with a thickness of ~ 30 μm at the centre. These thin foils were further thinned by an Ar-ion mill until a small hole formed in the centre. A cold stage, cooled by liquid N_2, was used to avoid undesirable thermal effects on samples by argon bombardment during the ion-milling process. Because these thin foils were also used for microchemistry studies, they were not mounted on Cu ovals in order to avoid Cu contamination during the ion-milling process. Generally, thin foils with diameters normal to the fibre axis were too weak to be prepared, and only those samples with disc diameter parallel to the fibre axis were successfully prepared. The thin specimens were not coated with an electrically conducting C coating on their surfaces, as it would effect the EDS analysis of the amorphous C layer in the interfacial regions. The charging effect on these thin foils from the electron beam during TEM microstructure studies was minimized due to the semiconducting nature of the SiC fibres.

The TEM was operated at 200 kV and microchemistry analysis of the fibre, interfacial zones, and matrix of the composite was conducted using a computer-linked windowless EDS facility, which allowed detection of all elements heavier than Be (including C). The spatial resolution of the electron beam for EDS analysis was approximately 30 nm, which is smaller than the thickness of the fibre/matrix interfacial layer.

3. Results and discussion

LAS II composites exhibited the highest flexural strength and fracture toughness, K_{IC}, of the fabricated composites in the previous study [8] (Table I). Fig. 1 shows the interfacial microstructure of this composite, which was hot pressed at 1300 °C for 15 min (pressure applied at 1000 °C). The high electron beam transmittance layer, ~ 100 nm thick, indicates that this region was composed of low atomic number elements, which was confirmed as a high C-content layer by EDS analysis (Fig. 1b). The selected-area diffraction pattern (SADP), in Fig. 2a, of this layer shows no ring pattern other than that related to the β-SiC fibre, implying that this layer was still in the amorphous state. Although, no features were observed in the SiC fibre (Fig. 1), three broadened rings in the SADP (Fig. 2b) imply that the fibres are of a fine polycrystalline form. EDS results (Fig. 1c) implied that a TaC particle layer was adjacent to the aforementioned C layer on the matrix side, which is verified by the SADP and dark-field image in Fig. 3. A crack between these two interfacial layers was also found, indicating that the low bonding strength between them caused a low interfacial shear strength between fibre and matrix. This in turn would lead to an increase in composite fracture toughness (Table I). Electron beam irradiation caused the vitrification of β spodumene solid solution (ss) in the matrix which thus appeared in the glassy state, with some dark particles corresponding to Ta_2O_5 [18, 19].

Fig. 4a illustrates the microstructure of the matrix portion of these composites. The ~ 3 μm grain of β spodumene ss (vitrified by the electron beam), is bordered by dark Ta_2O_5 particles [18, 19]. This grain size is ~ 30 times larger than that of a well heat-treated monolithic devitrified glass containing an identical amount of Ta_2O_5 [18]. The fast heating rate (~ 13 °C min^{-1}) of the hot-pressing schedule (as compared with 0.5 °C min^{-1} in the study of the monolithic glass ceramics [18]) for the densification of this composite would cause the matrix glass to form a limited number of nuclei for crystal growth of the major crystalline phase due to a short nucleation time, leaving adequate space for the limited number of β spodumene ss grains to grow to a larger size. The high soaking temperature (1300–1350 °C), and time, and slow furnace cooling of the hot-pressing schedule undoubtably enhanced the ultimate formation of β spodumene ss crystals over β quartz ss. Although some small Ta_2O_5 precipitates still remained in the centre region of β spodumene ss grains, much Ta_2O_5 segregated to the β spodumene ss grain boundaries and coalesced into larger grains (~ 0.5 μm). As the soaking temperature of hot pressing was increased to 1350 °C with the same holding time, the interfacial microstructure character did not change appreciably, however, the grain size of β spodumene ss increased to 5–7 μm, and most of the intergranular Ta_2O_5 precipitates diffused to the grain boundaries (Fig. 4b).

The interfacial microstructure of the LAS I composite (containing 2.0 mol % Ta_2O_5 dopant) is shown in Fig. 5. The SiC fibre, C-rich layer, and matrix

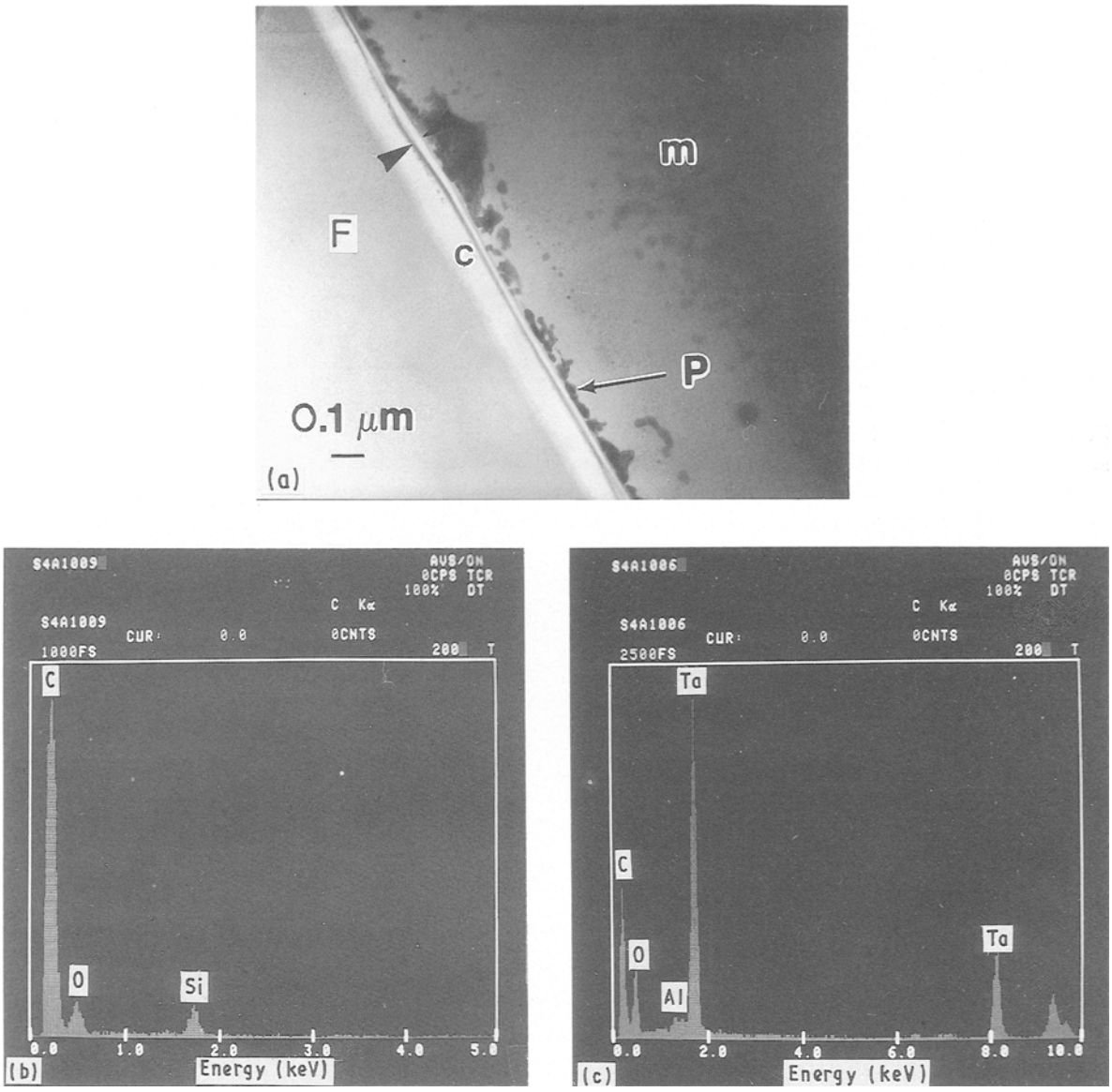

Figure 1 (a) Interfacial microstructure of the LAS II composite. F, SiC fibre; c, amorphous C-rich layer; m, matrix; P, TaC particles. (b, c) EDS results of C-rich layer, and TaC layer, respectively. Large arrows show a crack between the two interfacial layers.

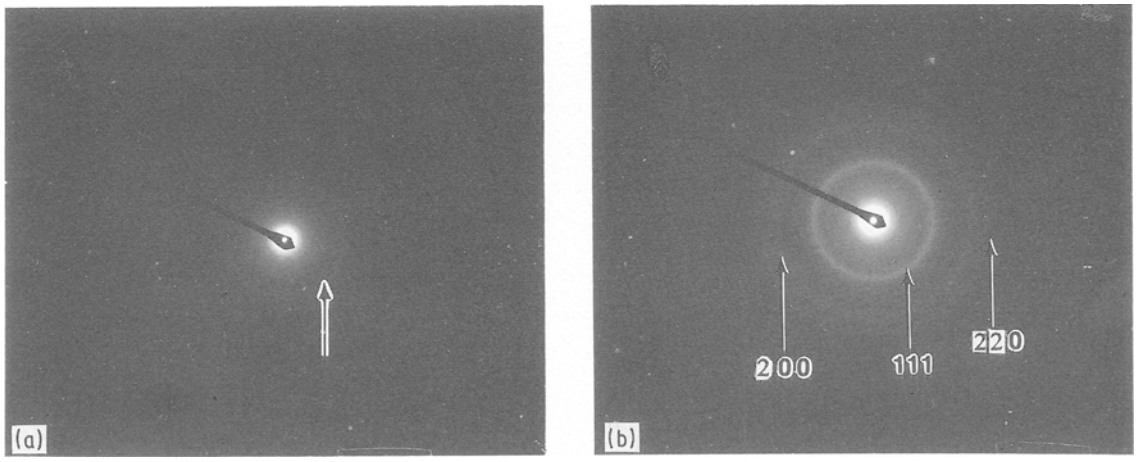

Figure 2 (a) SADP of a C-rich layer indicating a ring pattern (shown by arrow) from the SiC fibre, because the objective lens aperture is larger than the thickness of the C layer. (b) SADP taken from SiC fibre shows three rings corresponding to β SiC.

appear almost the same as those in LAS II composites, except that the density of TaC particles distributed adjacent to the C layer was much lower than that in the LAS II composites (Fig. 1). This was due to the diminished Ta content in the glass matrix available to form the TaC phase layer in the interfacial region. LAS I and LAS II composites had similar interfacial shear strengths between fibre and matrix [8]. This is

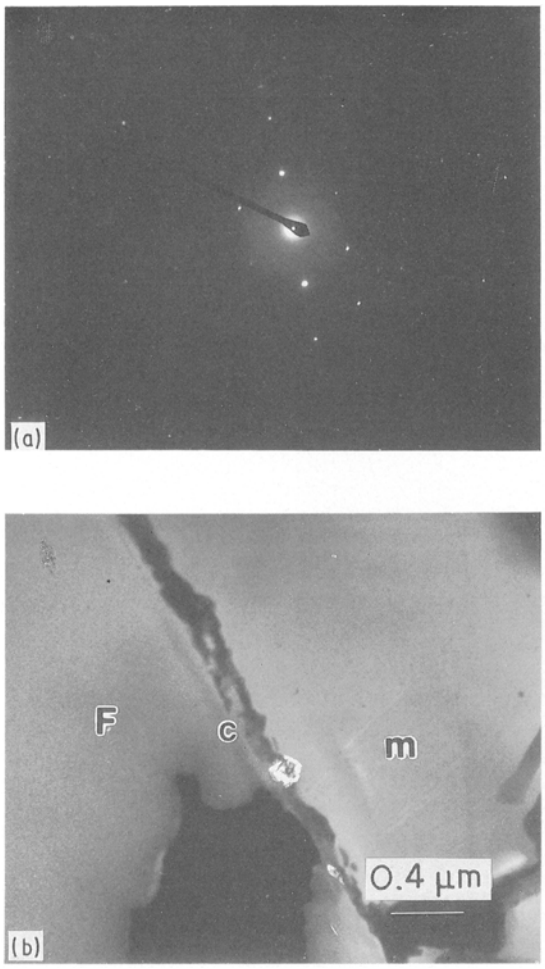

Figure 3 (a) SADP and (b) dark-field image of the TaC particle. The zone axis of the SADP is [0 1 1].

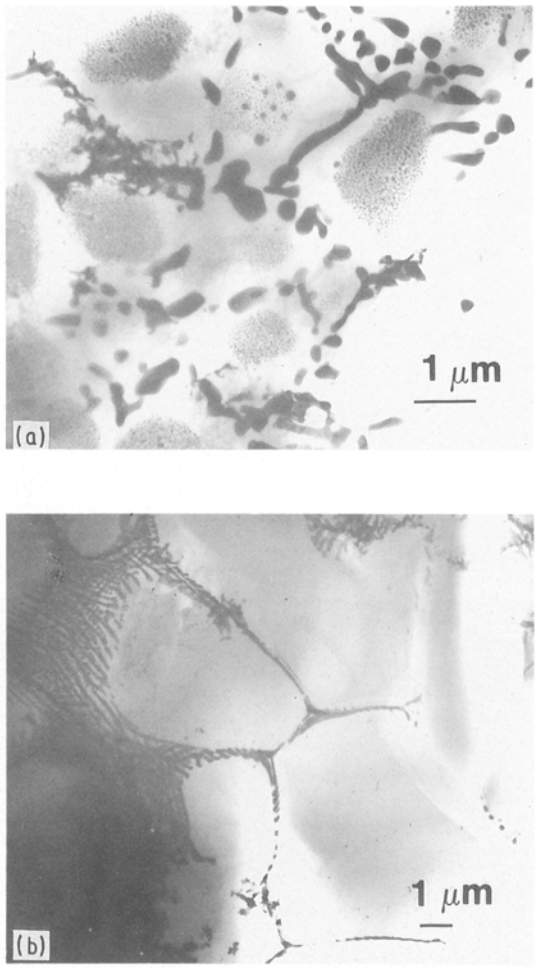

Figure 4 Matrix micrographs of the LAS II composites hot pressed at (a) 1300 °C, and (b) 1350 °C, for 15 min.

interpreted as being the result of the same thickness of C-rich layer in these composites. However, the lower Ta_2O_5 dopant concentration in the matrix constrained the formation of TaC, hence CO bubble formation was not suppressed. As a result, the flexural strength of the LAS I composites was lower than that of LAS II composites [7, 8, 11].

A C-rich layer of wider thickness (~ 170 nm) was observed in the LAS III composite, in its microchemistry, and confirmed by EDS analysis (Fig. 6). The larger thickness, compared with the LAS II composite, of this layer resulted from the higher hot-pressing temperature (1400 °C), because higher temperatures enhanced reactivity ($SiC + O_2 \rightarrow SiO_2 + C$) [11]. An NbC precipitate layer formed adjacent to the C-rich layer and was verified by EDS (Fig. 6b), SAD, and dark-field imaging (Fig. 7). A crack appeared and followed the interface between the C-rich layer and the NbC layer, detaching the SiC fibre from the matrix (Fig. 6). This crack was believed to form inadvertently, as in Fig. 1, during sample foil preparation, and suggests a low bonding strength between these two layers. This behaviour was also observed in a similar composite [10]. Because the SiC fibre debonded from the matrix at the interface between the C layer and the NbC layer, the thicker C layer, as compared with LAS I and II composites, apparently did not help to reduce

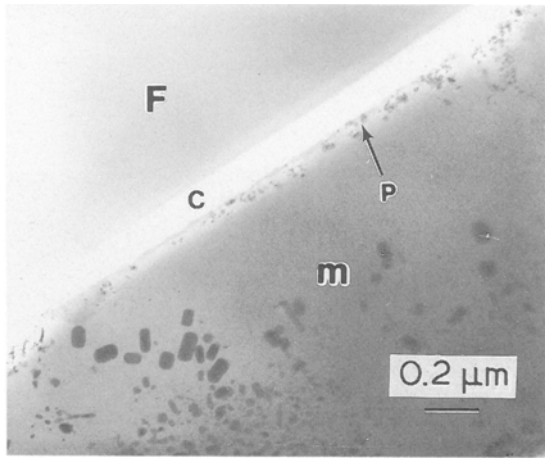

Figure 5 Interfacial microstructure of the LAS I composite. The C layer is about 100 nm thick. The density of TaC particles is much lower compared to the LAS II composite.

the interfacial shear strength between fibre and matrix in the LAS III composite [8]. The larger shear strength ~ 12.5 MPa, might have resulted from the higher hot-pressing temperature leading to compressive matrix/fibre stresses via thermal expansion mismatch between the fibre and matrix (NbC layer).

Fig. 8a shows the microstructure of the interfacial region in the LAS IV composite. A relatively thin

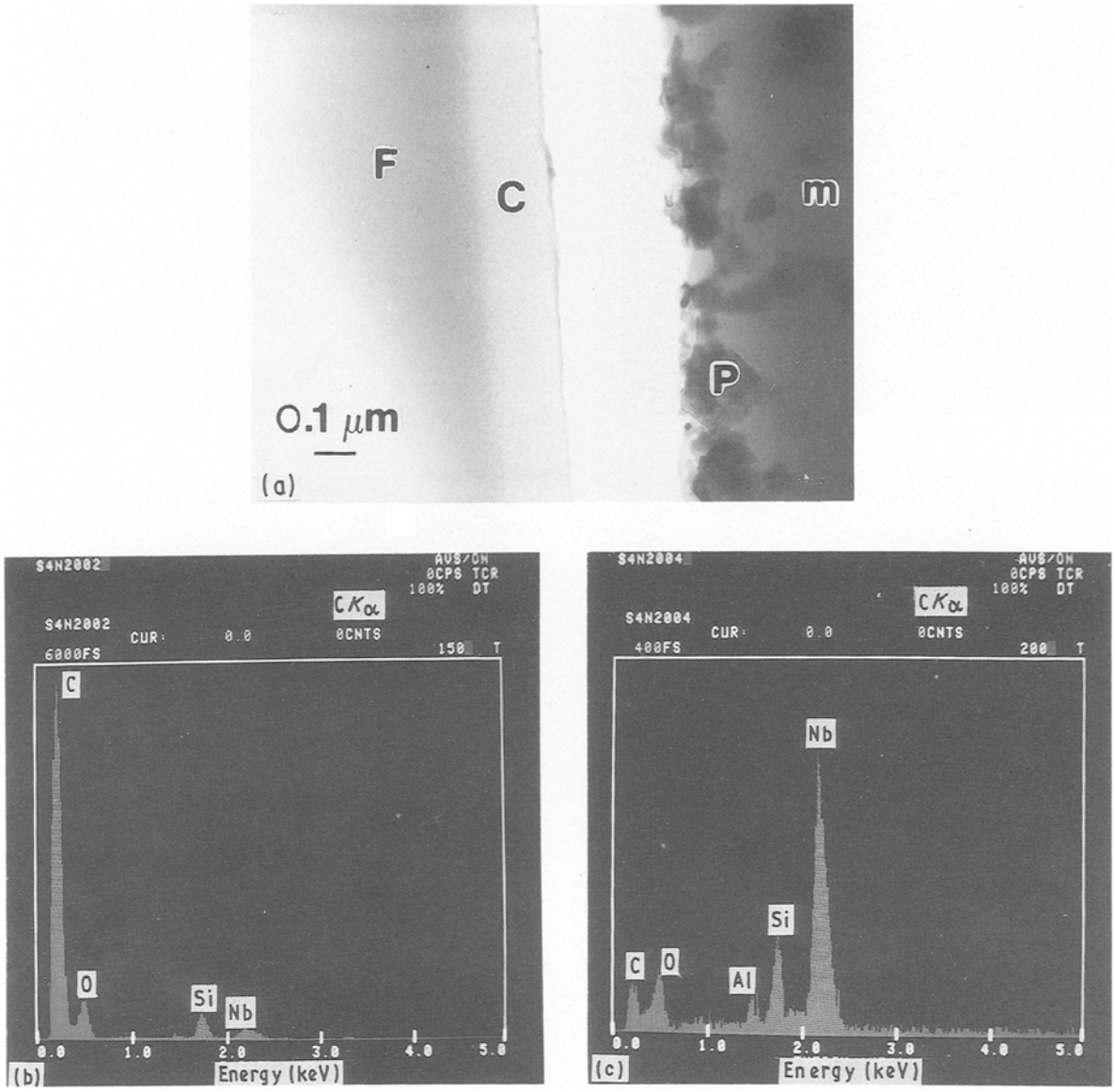

Figure 6 (a) Micrograph of LAS III composite. F, SiC fibre; c, C-rich layer; m, matrix; P, NbC particle layer. (b) EDS results of the C-rich layer, (c) EDS of the NbC particle layer.

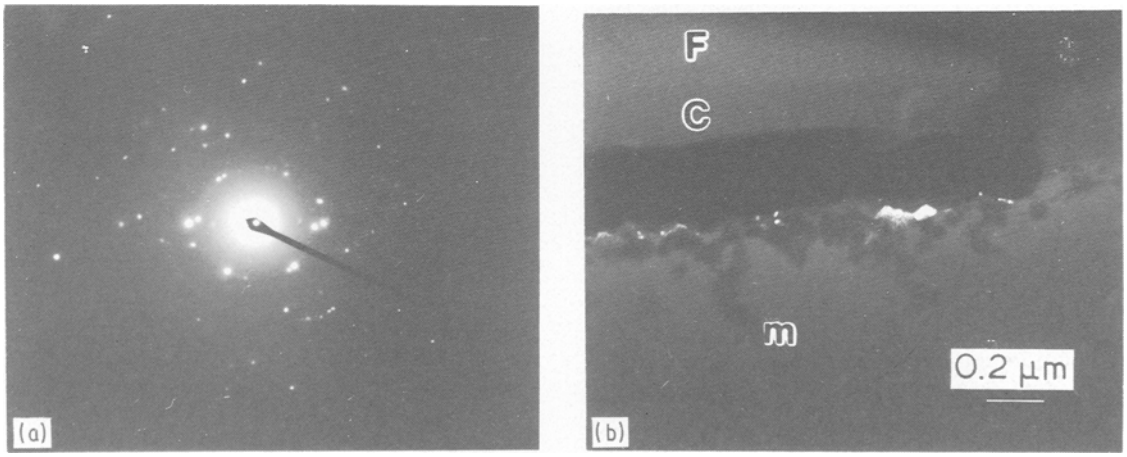

Figure 7 (a) SADP and (b) dark-field image of NbC particle. The zone axis of the SADP of the NbC particle is [0 1 1].

(~ 70 μm) C-rich layer was observed, confirmed by EDS results (Fig. 8c). Another layer of TiC precipitates next to the C-rich layer was found and identified by the micro-diffraction pattern in Fig. 8b and EDS analysis in Fig. 8d. Unlike the LAS II and LAS III composites, the bonding strength between the C-rich layer and the TiC layer was so strong that cracks would propagate through the matrix and fibres, and

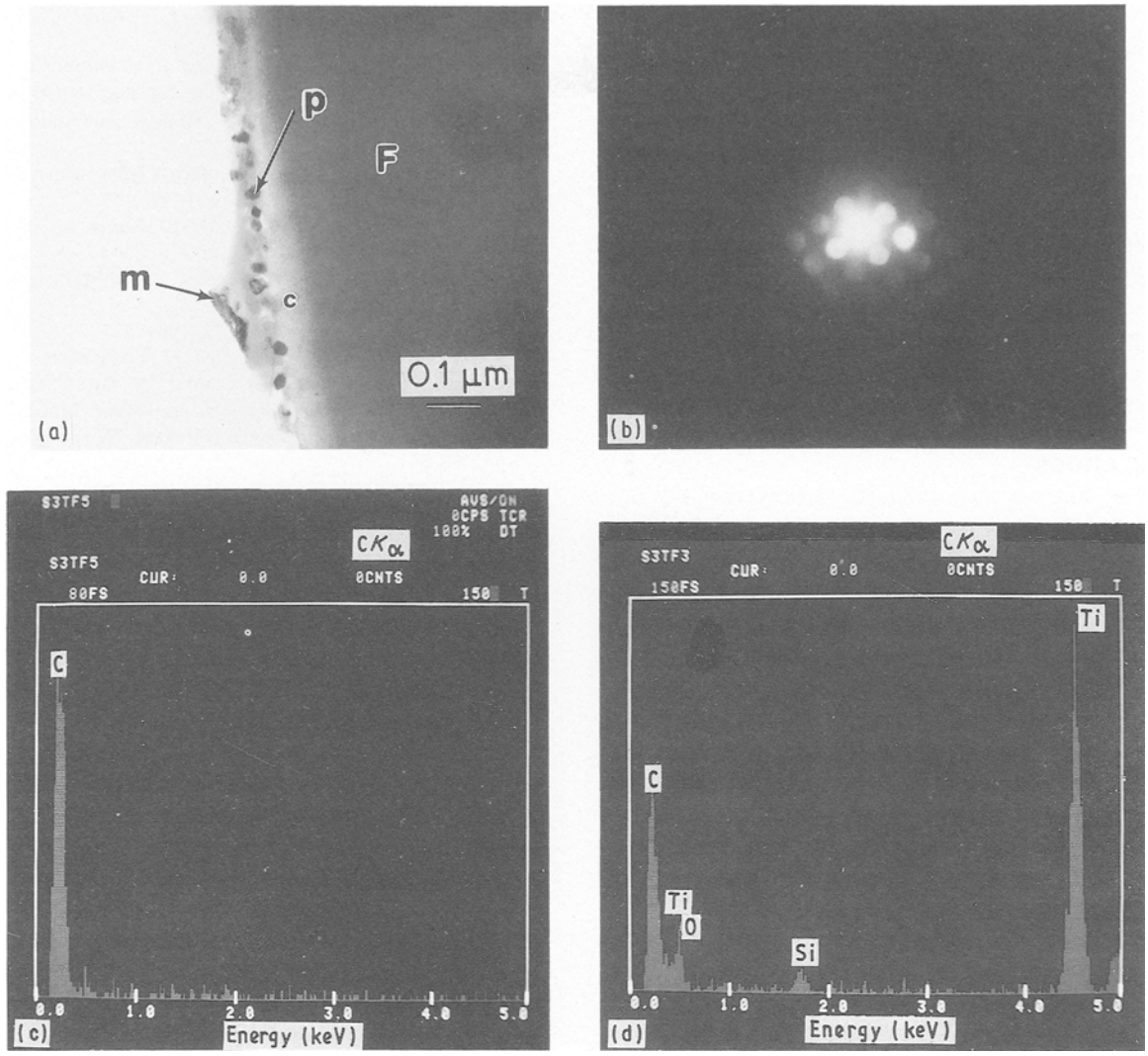

Figure 8 (a) Interfacial microstructure of the LAS IV composite. F, SiC fibre; c, C-rich layer; P, TiC particle layer; m, matrix. (b) Microdiffraction pattern of a TiC particle in the interfacial layer on the [0 0 1] zone axis. (c, d) EDS results show the C-rich layer, and TiC particle layer, respectively.

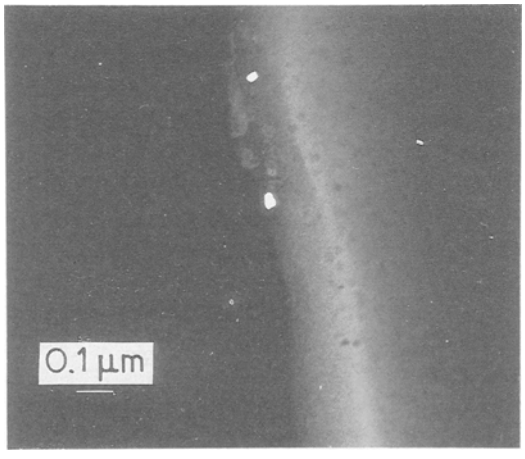

Figure 9 Dark-field image of TiC particles within the SiC fibre.

not between these two layers. Thus, high interfacial shear strength and low fracture toughness was observed in the LAS IV composites (Table I). Fig. 9 shows that some TiC precipitates formed inside the SiC fibre which would be expected to reduce the mechanical strength of the fibres, leading to the observed decrease in the flexural strength of the LAS IV composite.

4. Conclusion

An amorphous C-rich layer, 70–170 nm thick, was observed in the interfacial region of the investigated composites. A second interfacial layer, consisting of TaC or NbC particles, formed next to this C layer on the matrix side in the LAS II and LAS III composites. Low bonding strength between these two interfacial layers caused crack blunting which, in turn, passed in a direction parallel to the fibre axis. This mechanism led to fibre debonding and fibre pull-out, thus enhancing composite toughness. 2 mol% Ta_2O_5 dopant in the matrix was inadequate to form TaC particles in the interfacial region and caused a decrease in flexural strength of the LAS I composite. The formation of a TiC interfacial layer caused the high bonding strength between the SiC fibre and matrix leading to the low fracture toughness of the LAS IV composite. The TiC precipitation inside the SiC fibres caused a decrease in flexural strength of the LAS IV composite. The grain size of β spodumene ss in the composite matrix was

relatively large, 3–7 μm, due to the fast heating rate during the hot-pressing schedule. Ta_2O_5 and Nb_2O_5 were rejected to β spodumene ss grain boundaries during the composite densification process.

Acknowledgements

This work was supported by the New York State Center for Advanced Ceramic Technology at Alfred University, Alfred, NY, Contract no. 12-76-75. The authors thank Ms Y. Berta for her instructive opinions and guidance in the microstructure investigation by transmission electron microscopy.

References

1. K. M. PREWO, *Amer. Ceram. Soc. Bull.* **68** (1989) 395.
2. D. BELITSKUS, *Materials and Design* **10** (1989) 2.
3. K. K. CHAWLA, "Composite Materials, Science and Engineering" (Springer-Verlag, New York, 1987) pp. 135–50.
4. J. J. MECHOLSKY, *Amer. Ceram. Soc. Bull.* **68** (1988) 367.
5. K. M. PREWO, J. J. BRENNAN and G. K. LAYDEN, *ibid.* **65** (1986) 305.
6. K. M. PREWO, in "Procedings of the 21st University Conference on Ceramic Science", Pennsylvania State University, July 1985, pp. 529–47.
7. J. J. BRENNAN and K. M. PREWO, *J. Mater. Sci.* **17** (1982) 2371.
8. J. Y. HSU and R. F. SPEYER, *ibid.* to be published.
9. J. J. BRENNAN, in "Proceedings of the 21st University Conference on Ceramic Science", Pennsylvania State University, July 1985, pp. 549–60.
10. R. CHAIM and A. H. HEUER, *Advn. Ceram. Mater.* **2** (1987) 154.
11. R. F. COOPER and K. CHYUNG, *J. Mater. Sci.* **22** (1987) 3148.
12. P. G. CHARALAMBIDES and A. G. EVANS, *J. Amer. Ceram. Soc.* **72** (1989) 746.
13. M. D. THOULESS *et al.*, *ibid.* **72** (1989) 525.
14. A. G. EVANS and M. Y. HE, *ibid.* **72** (1989) 2300.
15. T. W. COYLE, H. M. CHAN and U. V. DESHMUKH, in "Interfaces in Polymer, Ceramic, and Metal Matrix Composite", edited by H. Ishida (Elsevier, New York, 1988) pp. 489–501.
16. K. M. PREWO, *J. Mater. Sci.* **21** (1986) 3590.
17. *Idem., ibid.* **22** (1987) 2695.
18. J. Y. HSU and R. F. SPEYER, *J. Amer. Ceram. Soc.* **72** (1989) 2334.
19. *Idem., ibid.* **73** (1990) 3585.
20. *Idem., ibid.* **74** (1991) 395.

Received 16 July
and accepted 30 November 1990